



HAL
open science

Atom chips and one-dimensional Bose gases

Isabelle Bouchoule, N. J. van Druten, Christoph I Westbrook

► **To cite this version:**

Isabelle Bouchoule, N. J. van Druten, Christoph I Westbrook. Atom chips and one-dimensional Bose gases. J. Reichel and V. Vuletic. Atom chips, Wiley-VCH Verlag GmbH, pp.331, 2011. hal-00354920v2

HAL Id: hal-00354920

<https://hal.science/hal-00354920v2>

Submitted on 23 Jan 2009

HAL is a multi-disciplinary open access archive for the deposit and dissemination of scientific research documents, whether they are published or not. The documents may come from teaching and research institutions in France or abroad, or from public or private research centers.

L'archive ouverte pluridisciplinaire **HAL**, est destinée au dépôt et à la diffusion de documents scientifiques de niveau recherche, publiés ou non, émanant des établissements d'enseignement et de recherche français ou étrangers, des laboratoires publics ou privés.

Atom chips and one-dimensional Bose gases

I. Bouchoule¹, N.J. van Druten², C. I. Westbrook¹

1: Laboratoire Charles-Fabry, CNRS UMR 8501, Institut d'Optique, Palaiseau, France

2: Van der Waals-Zeeman Instituut, Universiteit van Amsterdam, The Netherlands

January 26, 2009

Contents

1	Introduction	2
2	Regimes of 1D gases	2
2.1	Strongly versus weakly interacting regimes	4
2.2	Nearly ideal gas regime	6
2.3	Quasi-condensate regime	9
2.3.1	Density fluctuations	10
2.3.2	Phase fluctuations	11
2.4	Exact thermodynamics	13
3	1D gases in the real world	16
3.1	Transverse trapping and nearly 1D Bose gases	16
3.2	Applying 1D thermodynamics to a 3D trapped gas	17
3.3	Longitudinal trapping	18
3.3.1	Local density approximation	18
3.3.2	Validity of the local density approximation	19
3.4	3D physics versus 1D physics	19
4	Experiments	21
4.1	Failure of the Hartree-Fock model	21
4.2	Yang-Yang analysis	22
4.3	Measurements of density fluctuations	23
4.3.1	A local density analysis	25
4.3.2	Ideal gas regime : observation of bunching	25
4.3.3	Quasi-condensate regime: saturation of atom number fluctuations	28
5	Conclusion	29

1 Introduction

As this volume indicates, the technology of atom chips is currently enjoying great success for a large variety of experiments on degenerate quantum gases. Because of their geometry and their ability to create highly confining potentials, they are particularly well adapted to realizing one dimensional (1D) situations [1, 2, 3, 4, 5, 6, 7, 8, 9]. This characteristic has contributed to a revival of interest in the study of 1D Bose gases with repulsive interactions, a system which provides a vivid example of an exactly solvable quantum many-body system [10, 11, 12]. The quantum many-body eigenstates [10, 11] and thermodynamics [12] can be calculated without resorting to approximations. In addition, the 1D Bose gas shows a remarkably rich variety of physical regimes (see Fig. 1) that are very different both from those found in 2D and in 3D. One dramatic example of the difference is the tendency for a 1D Bose gas to become more *strongly* interacting as its density *decreases* [10]. Finally, and in a more practical vein, a good understanding of its behavior is relevant for guided-wave atom lasers [13] and trapped-atom interferometry [14]. Because of the effects of interactions, the analogy to the manipulation of light in single mode fibers needs to be examined carefully.

An atom chip is not the only means of producing a 1D Bose gas. Optical trapping has been used to generate similarly elongated trap geometries. In particular, a 2D optical lattice can be used to generate a 2D array of 1D traps [15, 16, 17, 18, 19]. Because of the massively parallel nature of this system, it is possible to work with only a few atoms per tube, and still get a sizeable signal per experimental cycle. Thus, the strongly interacting regime alluded to above can be reached. This regime has yet to be reached with an atom chip. But as we will show here, a key feature of atom chips is that they produce individual samples in which one does not intrinsically average over many realizations. Fluctuation phenomena are therefore readily accessible, an aspect which we will treat later in this chapter.

In the following we first give an introduction to the various regimes of the homogeneous 1D Bose gas, with particular emphasis on the behavior of the density profiles and the density fluctuations in the context of approximate models. Then we will discuss the exact solution and how it differs from the approximations. Next, we discuss some of the important issues involved in realizing 1D gases in a 3D trap. Finally, we describe a series of experiments performed in Orsay and Amsterdam using atom chips to explore and illustrate features of the 1D Bose gas.

2 Regimes of one-dimensional gases

First, we review some theoretical results concerning the one-dimensional Bose gas with repulsive interactions. Most of these results are derived in Refs. [10, 12, 20, 21, 22, 23, 24]. Here we will concentrate on intuitive arguments, and the reader is referred to the above references for more

careful demonstrations. The system is described by the Hamiltonian

$$H = -\frac{\hbar^2}{2m} \int dz \psi^\dagger \frac{\partial^2}{\partial z^2} \psi + \frac{g}{2} \int dz \psi^\dagger \psi^\dagger \psi \psi, \quad (1)$$

where ψ is the field operator in second quantization, and g is the coupling constant characterizing the interactions between particles. From this coupling constant, one can deduce an intrinsic length scale related to the interactions,

$$l_g = \frac{\hbar^2}{mg}, \quad (2)$$

as well as an energy scale:

$$E_g = \frac{mg^2}{2\hbar^2} = \frac{\hbar^2}{2ml_g^2}. \quad (3)$$

In thermal equilibrium, the gas is described by the temperature T and the linear atomic density n . Rescaling these two quantities by the intrinsic scales introduced above, and setting Boltzmann's constant equal to unity (i.e., measuring temperature in units of energy) we find that the properties of the gas are functions of the dimensionless quantities

$$t = \frac{T}{E_g}, \quad (4)$$

and

$$\gamma = \frac{mg}{\hbar^2 n} = \frac{1}{nl_g}, \quad (5)$$

the latter being the famous Lieb-Liniger parameter [10].

It is useful to also introduce two other relevant scales, namely the thermal de Broglie wavelength,

$$\lambda_{dB} = \hbar \sqrt{\frac{2\pi}{mT}} = l_g \sqrt{\frac{4\pi}{t}}, \quad (6)$$

and the quantum degeneracy temperature

$$T_d = \frac{\hbar^2 n^2}{2m} = \frac{E_g}{\gamma^2}. \quad (7)$$

In the above (t, γ) parametrization, quantum degeneracy ($T \approx T_d$, or equivalently $n\lambda_{dB} \approx 1$) is reached around

$$t \approx \frac{1}{\gamma^2}. \quad (8)$$

The thermal equilibrium for the hamiltonian of Eq. (1) has been extensively studied theoretically [12,22]. Without going into great detail however, we can present some important features of this system. Several regimes may be identified in the parameter space (γ, t) , as sketched in Fig. 1. We begin by noting that the region $\gamma \gg 1, t \ll 1$ (dark grey area) defines a strongly interacting

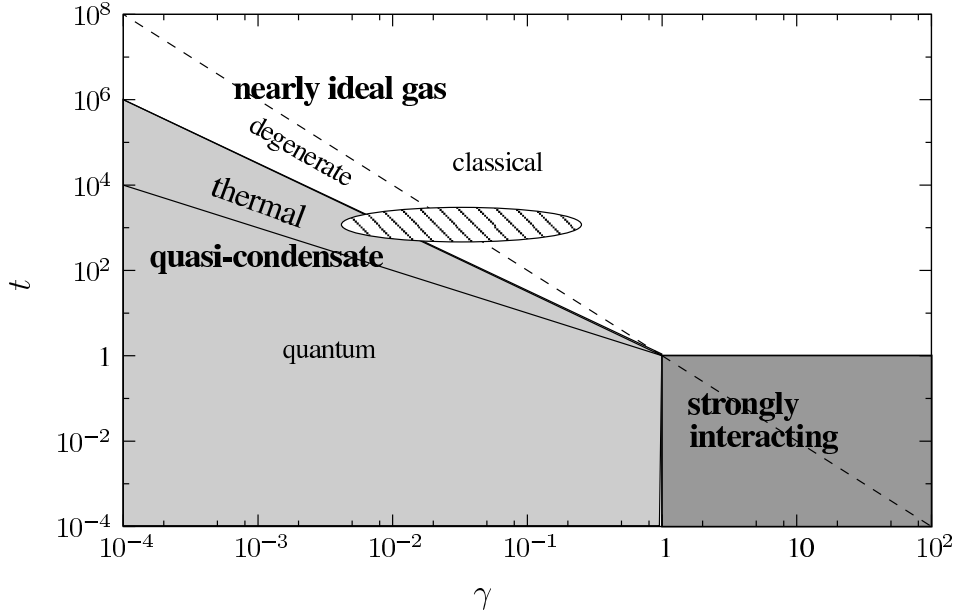


Figure 1: *Physical regimes of a 1D Bose gas with repulsive contact interactions in the parameter space (γ, t) , adapted from [22]. The dashed diagonal line separates the degenerate and nondegenerate gases. The strongly interacting regime is shown in dark grey. The weakly interacting regime is divided into the nearly ideal gas regime (also called decoherent regime) shown in white and the quasicondensate regime shown in light grey. Note that the nearly ideal gas can be degenerate. The quasicondensate regime is divided into the thermal and quantum regimes. The lines represent smooth (and often wide) crossovers rather than phase transitions. The crossovers are given in Eqs. (10), (11), (8), (25) and (41). The dashed area shows the parameter space investigated in the experiments presented in this chapter.*

regime that occurs at low density and low temperature, often referred to as the Tonks-Girardeau gas [25, 26, 20].

In the weakly interacting regime, $\gamma < 1$, several sub-regimes are identified. These are the regimes which to date have been accessible in atom chip experiments, and we shall elaborate further on their nature in the discussion below. The two main regimes are the nearly ideal gas regime (white area) and the quasi-condensate regime (light grey area). Each one permits an approximate description that we present later in this section and which allows the identification of sub-regimes. For the moment we simply wish to emphasize that no phase transition occurs in the 1D Bose gas and that all the boundaries represent smooth (and often broad) crossovers in behavior.

2.1 Strongly versus weakly interacting regimes

We first comment on the distinction between strong and weak interactions. Following the approach of Ref. [20], we study the scattering wave function of two atoms interacting via the potential $g\delta(z_1 - z_2)$, where z_1 and z_2 are the position of the two atoms. For this, we consider the

wave function ψ in the center-of-mass frame, with reduced mass $m/2$ and subject to the potential $g\delta(z)$. The effect of the potential is described by the continuity condition

$$\frac{\partial}{\partial z}\psi(0_+) - \frac{\partial}{\partial z}\psi(0_-) = \frac{mg}{2\hbar^2}\psi(0) \quad (9)$$

where 0_+ (0_-) denotes the limit when z goes to zero through positive (negative) values. Let us consider the scattering solution for an energy $E = \hbar^2k^2/m$. Since we consider bosons, we look for even wave functions of the form $\cos(k|z| + \phi)$. The continuity conditions give ϕ and thus the value $\psi(0)$. We find then that the energy E_g given by Eq. (3) is the relevant energy scale and that for $E \ll E_g$, $\psi(0)$ is close to zero, while, for $E \gg E_g$, $\psi(0)$ is close to one, as illustrated in Fig. 2.

The above results hold for a gas of particles since the continuity relation (9) holds for the many-body wavefunction when two atoms are close to the same place. Thus, as long as the typical energy of the particles is much lower than E_g , the many-body wavefunction vanishes when two particles are at the same position: the gas is then in the strongly interacting, or Tonks-Girardeau regime. The vanishing of the wave function when two particles are at the same place mimics the Pauli exclusion principle and the gas acquires some similarities with a gas of non interacting fermions. More precisely, in this strong interaction regime, the available wave functions of the many body problem are, up to a symmetrization factor, the wave functions of an ideal Fermi gas [26]. Since the wave function vanishes when two atoms are at the same place, the energy of the system is purely kinetic energy and the eigen energies are those of the Fermi system. Thus the 1D strongly interacting Bose gas and the ideal 1D Fermi gas share the same energy spectrum. This implies in particular that all thermodynamic quantities are identical for both systems.

To identify the parameter space of the strongly interacting regime, we suppose the gas to be strongly interacting and then require that the typical energy of the atoms be smaller than E_g . To estimate the typical energy per atom, we use the Bose-Fermi mapping presented above. If the gas is degenerate, the temperature is smaller than the degeneracy temperature T_d , Eq. (7), and T_d corresponds to the "Fermi" energy of the atoms. The typical atom energy is therefore T_d and it is of order E_g if

$$\gamma \simeq 1. \quad (10)$$

The strongly interacting regime thus requires $\gamma \gg 1$. If the gas is non degenerate, the typical energy of the equivalent Fermi gas is T and interactions become strong when $T = E_g$ or

$$t \simeq 1. \quad (11)$$

We then find that the gas is strongly interacting for $t \ll 1$.

The condition (10) is often derived using the following alternative argument, valid at zero temperature. At zero temperature, there are two extremes for the possible solutions for the wave function $\psi(z_1, z_2, \dots)$. As seen in Fig. 2, either the wave function vanishes when two atoms are at the same place, or the wave function is almost uniform, corresponding to the strongly and weakly interacting configurations respectively. In the weakly interacting configuration, the kinetic energy is negligible and the interaction energy per particle, of the order of gn , determines

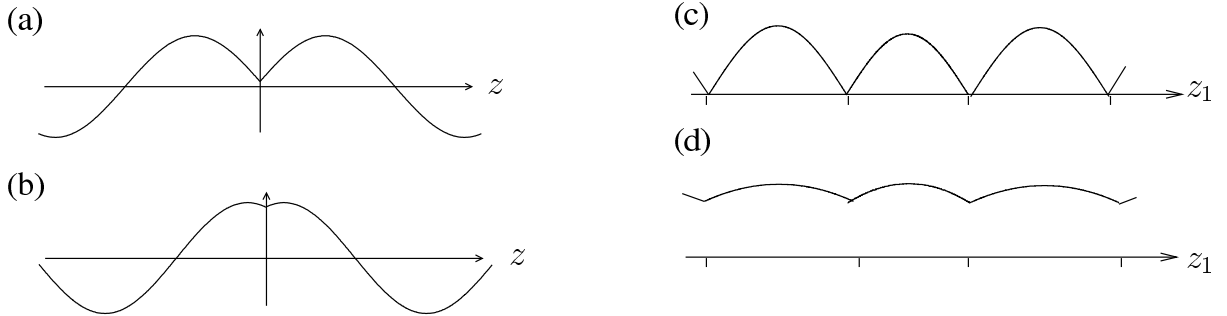


Figure 2: *Strong interaction versus weak interaction regime. We show the wave function in the center-of-mass frame of two atoms for (a) strong interactions, scattering energy E much smaller than $E_g = mg^2/2\hbar^2$ and (b) weak interactions, E much larger than E_g . We also plot the wave function $\psi(z_1, z_2, z_3, \dots)$ for given positions of z_2, z_3, \dots in (c) the strongly interacting regime and (d) the weakly interacting regime.*

the total energy. In the strongly interacting configuration, on the other hand, the interaction energy vanishes while the typical kinetic energy per particle is $\hbar^2 n^2/m$. Comparing these two energies, we find that the strongly interacting configuration is favorable only for $\gamma > 1$.

2.2 Nearly ideal gas regime

At sufficiently high temperatures, interactions between atoms have little effect and the gas is well described by an ideal Bose gas. In Ref. [22], this regime was referred to as the "decoherent regime"; We will call it the (nearly) ideal Bose gas regime. A 1D ideal Bose gas at thermal equilibrium is well described using the grand canonical ensemble, introducing the chemical potential μ . All properties of the gas are calculated using the Boltzmann law which states that, for a given one-particle state of momentum $\hbar k$, the probability to find N atoms in this state is proportional to $e^{-(\hbar^2 k^2/(2m) - \mu)N/T}$; note that $\mu < 0$ in this description. In the following, we use a quantization box of size L (tending to infinity in the thermodynamic limit) and periodic boundary conditions so that the available states are the momentum states with momentum $k = 2\pi j/L$ where j is an integer.

Let us first consider the linear gas density. From the Boltzmann law, we find that the mean population is the Bose distribution

$$\langle n_k \rangle = \frac{1}{e^{(\hbar^2 k^2/(2m) - \mu)/T} - 1}. \quad (12)$$

The atom number, and thus the linear density, is obtained by summing the population over the states and one finds

$$n = \frac{1}{\lambda_{dB}} g_{1/2}(e^{\mu/T}), \quad (13)$$

where $g_{1/2}(x)$ is one of the Bose functions

$$g_n(x) = \sum_{l=1}^{\infty} \frac{x^l}{l^n}, \quad (14)$$

also known as the polylogarithmic functions [27, 28]. Unlike in 3D systems, where the excited-state density is given by $\rho_e = g_{3/2}(e^{\mu/T})/\lambda_{dB}^3$ in this approach [27], no saturation of the excited states occurs (the function $g_{1/2}$ diverges as $\sqrt{-\pi T/\mu}$ as $\mu \rightarrow 0$ from below, whereas $g_{3/2}(1) = 2.612$ is finite): in the thermodynamic limit no Bose-Einstein condensation is expected and the gas is well described by a thermal gas at any density.

Two asymptotic regimes may be identified: the non degenerate regime for which $-\mu \gg T$ and $\hbar^2 n^2/m \ll T$ and the degenerate regime for which $-\mu \ll T$ and $\hbar^2 n^2/m \gg T$. In the non degenerate regime, the linear density is well approximated by the Maxwell-Boltzmann formula

$$n = \frac{1}{\lambda_{dB}} e^{\mu/T}, \quad (15)$$

In this regime $n\lambda_{dB}$ is much smaller than unity. In the degenerate regime, the states of energy much smaller than T are highly occupied and the linear density is given by

$$n = \frac{T}{\hbar} \sqrt{\frac{m}{-2\mu}} \quad (16)$$

This density is much larger than $1/\lambda_{dB}$, *i.e.* $n\lambda_{dB} \gg 1$.

As we will discuss in the experimental section, fluctuations are also very important for characterizing the gas. It is thus instructive to consider the correlation functions. The normalized one body correlation function is $g^{(1)}(z) = \langle \psi^\dagger(0)\psi(z) \rangle / n$, where ψ is the field operator in the second quantization picture. Using the expansion of the field operator in the plane wave basis $\psi(z) = \sum_k a_k e^{-ikz} / \sqrt{L}$ where a_k is the annihilation operator for the mode k , we find $g^{(1)}(z) = \sum_k \langle n_k \rangle e^{-ikz} / (Ln)$. Here $n_k = a_k^\dagger a_k$ is the atom number operator for the mode k . Simple analytical expressions are found in the nondegenerate and highly degenerate limits. In the non degenerate limit ($-\mu \gg T$ or, equivalently $n \ll 1/\lambda_{dB}$), we find

$$g^{(1)}(z) \simeq e^{-\frac{z^2}{4\pi\lambda_{dB}^2}}. \quad (17)$$

As the gas becomes more degenerate, the correlation length increases and, in the degenerate regime ($-\mu \ll T$ or, equivalently $n \gg 1/\lambda_{dB}$), we find

$$g^{(1)}(z) \simeq e^{-\frac{mTz}{\hbar^2}} = e^{-\frac{2\pi z}{n\lambda_{dB}^2}}. \quad (18)$$

In this regime the correlation length, about $n\lambda_{dB}^2$, is much larger than the de Broglie wavelength (and the mean interparticle distance $1/n$) since $\lambda_{dB} \gg 1/n$.

Next we consider the normalized density-density or two body correlation function

$$g^{(2)}(z) = \langle \psi^\dagger(z)\psi^\dagger(0)\psi(0)\psi(z) \rangle / n^2. \quad (19)$$

This function is proportional to the probability of finding an atom at position z and at position $z = 0$. It is given by

$$n^2 g^{(2)}(z) = \sum_{k_1 k_2 k_3 k_4} \langle a_{k_1}^\dagger a_{k_2}^\dagger a_{k_3} a_{k_4} \rangle e^{ik_1 z} e^{-ik_4 z} / L^2. \quad (20)$$

Using Bose commutation relations and the fact that, since atoms do not interact, different momentum state populations are uncorrelated, the sum simplifies to:

$$n^2 g^{(2)}(z) = \sum_{k_1 \neq k_2} \langle n_{k_1} \rangle \langle n_{k_2} \rangle (1 + e^{i(k_1 - k_2)z}) / L^2 + \sum_k \langle a_k^\dagger a_k^\dagger a_k a_k \rangle / L^2. \quad (21)$$

In the last term, the commutation relations give: $\langle a_k^\dagger a_k^\dagger a_k a_k \rangle = \langle n_k^2 \rangle - \langle n_k \rangle$, and in thermal equilibrium one has:

$$\langle n_k^2 \rangle = \langle n_k \rangle + 2\langle n_k \rangle^2. \quad (22)$$

Therefore we find:

$$g^{(2)}(z) = 1 + |g^{(1)}(z)|^2, \quad (23)$$

a result which one can also obtain directly from Wick's theorem [29]. Equation (23) means that the probability of finding atoms within less than a correlation length in a thermal Bose gas is twice that of finding two atoms far apart. This phenomenon is often referred to as "bunching" and has been observed in cold atoms in several experiments [30, 31, 32]. Bunching is closely related to density fluctuations. As one can see from Eq. (22), in a thermal gas, fluctuations in the occupation of a single quantum state, $\delta n_k^2 = \langle n_k^2 \rangle - \langle n_k \rangle^2$, show a "shot noise" term, $\langle n_k \rangle$ and an "excess noise" term, $\langle n_k \rangle^2$. The density fluctuation experiment described later in this chapter has demonstrated this behavior.

Validity of the ideal gas treatment. The two body correlation function has been used to characterize the crossover between the ideal gas and quasi-condensate regimes [22]. When interactions become important, they impose an energy cost on density fluctuations and the latter tend to smooth out. This amounts to a reduction in the value of $g^{(2)}(0)$. In the quasi-condensate regime which we discuss in the next section, the bunching effect is absent and $g^{(2)}(0)$ is close to unity. The ideal Bose gas description fails when the typical interaction energy per particle gn is not negligible compared to $-\mu$. Using Eq. (16) one finds that the ideal Bose gas description fails when the temperature is no longer much smaller than the crossover temperature, which we define as

$$T_{co} \simeq T_d \sqrt{\gamma}. \quad (24)$$

Using the reduced dimensionless temperature $t = T/E_g$, this can be written as

$$t_{co} \simeq \frac{1}{\gamma^{3/2}}. \quad (25)$$

This line separates the nearly ideal gas regime from the quasi-condensate regime in Fig. 1. Note that, in terms of chemical potential, the domain of validity of the ideal gas model is $-\mu \gg \mu_{co}$ where we define the crossover chemical potential as

$$\mu_{co} = \frac{T}{t^{1/3}}. \quad (26)$$

In making this estimate, we have assumed that the gas is degenerate at the crossover. From Eq. (24), one can see that if one is in the weakly interacting regime ($\gamma \ll 1$) this assumption

is indeed true. The experiments described below confirm that one can observe the effects of degeneracy before the onset of the reduction of density fluctuations.

A precursor of the reduction of density fluctuations is shown by a perturbative calculation valid in the nearly ideal gas regime which gives, to lowest order in g [22],

$$g^{(2)}(0) \simeq 2 - 4(T_{co}/T)^2. \quad (27)$$

To accurately treat the crossover regime however, it is necessary to make use of the exact solution to the 1D Bose gas model. The exact solution in the crossover regime is discussed in Sec. 2.4.

The correlation lengths of the gas are important parameters of the gas that will be used in the following to estimate the validity criteria of the local density approximation. In the degenerate regime, the correlation length is $l_c \simeq n\lambda_{dB}^2$ (see Eq. (18)). Using Eq. (24), we find that, close to the crossover, the correlation length of the gas is close to the healing length

$$\xi = \frac{\hbar}{\sqrt{mgn}}. \quad (28)$$

2.3 Quasi-condensate regime

On the other side of the crossover, *i.e.* for $T \ll T_{co}$, the bunching effect is entirely suppressed and the $g^{(2)}$ function is close to unity for any z . This regime is the quasi-condensate regime¹. In this section, we present a description of the gas, valid in the quasi-condensate regime. This description permits a simple estimate of the density fluctuations. We thus verify *a posteriori* that the quasi-condensate regime is obtained for $T \ll T_{co}$. We also give a simple calculation of phase fluctuations in the quasi-condensate regime.

In the quasi-condensate regime density fluctuations are strongly reduced compared to their value in an ideal Bose gas where the bunching effect is responsible for density fluctuations of the order of n^2 . In other words:

$$\delta n^2 \ll n^2 \quad (29)$$

In this regime, a suitable description is realized by writing the field operator as $\psi = e^{i\theta} \sqrt{n + \delta n}$ where the real number n is the mean density and the operator δn and the phase operator θ are conjugate: $[\delta n(z), \theta(z')] = i\delta(z - z')$. Note that the definition of a local phase operator is subtle and the condition Eq. (29) is not well defined since, because of shot noise, δn^2 is expected to diverge in a small volume. A rigorous and simple approach consists in discretizing the space so that in each cell a large number of atoms is present while the discretisation step is much smaller than the correlation length of density and phase fluctuations [33].

Following this prescription, one first minimizes the grand canonical Hamiltonian $H - \mu N$ with respect to n to obtain the equation of state

$$\mu = gn. \quad (30)$$

¹It is also called coherent regime since the $g^{(2)}$ function is close to unity, as in a coherent state. On the other hand, the first order correlation function still decays and so the gas is not strictly coherent in this sense. Within this terminology, the ideal Bose gas regime is called the decoherent regime [22].

To second order in δn , this is the correct expression of the chemical potential. This equality ensures that the Hamiltonian has no linear terms in δn and $\nabla\theta$. Linearizing the Heisenberg equations of motion in δn and $\nabla\theta$, we obtain [33]

$$\begin{cases} \hbar\partial\theta/\partial t = -\frac{1}{2\sqrt{n}}(-\frac{\hbar^2}{2m}\Delta + 2gn)\frac{\delta n}{\sqrt{n}} \\ \hbar\partial\delta n/\partial t = 2\sqrt{n}(-\frac{\hbar^2}{2m}\Delta)\theta\sqrt{n} \end{cases} \quad (31)$$

These equations are the so-called hydrodynamic equations. They are derived from a Hamiltonian quadratic in δn and $\nabla\theta$, that can be diagonalized using the Bogoliubov procedure [33]. It is not the purpose of this chapter to detail this calculation and to give exact results within this theory. We will simply give arguments that enable an estimate of the density fluctuations and of their correlation length. This estimate will then be used to check that $\delta n^2 \ll n^2$, as assumed in Eq. (29). We will show that this condition is the same as the condition $T \ll T_{co}$ where T_{co} given in Eq. (24). After that, we will give similar arguments to estimate the phase fluctuations. Since in the following we will study the gas properties versus the chemical potential, it is instructive to rewrite the condition $T \ll T_{co}$ in terms of chemical potential. Using Eq. (30), we find that the quasi-condensate regime is valid as long as $\mu \gg \mu_{co}$ where μ_{co} is given by Eq. (26).

2.3.1 Density fluctuations

To estimate the density fluctuations introduced by the excitations, it is convenient to divide the excitations in two groups: the excitations of low wave vector for which the phase representation is most appropriate and the excitations of high wave vector for which a particle point of view is most convenient.

In the following, we use the expansions on sinusoidal modes $\theta = \sum_{k>0} \sqrt{2}(\theta_{ck} \cos(kz) + \theta_{sk} \sin(kz))$ and $\delta n = \sum_{k>0} \sqrt{2}(\delta n_{ck} \cos(kz) + \delta n_{sk} \sin(kz))$. Here δn_{jk} and θ_{jk} are conjugate variables ($[\delta n_{jk}, \theta_{j'k'}] = (i/L)\delta_{jj'}\delta_{kk'}$) where j stands for c or s . For modes of small wave vector k , the excitations are phonons, or density waves, for which the relative density modulation amplitude $\delta n_{jk}/n$ is much smaller than the phase modulation amplitude θ_{jk} . In this case, the local velocity of the gas is given by $\hbar\nabla\theta/m$ and the kinetic energy term is simply $Ln\hbar^2k^2\theta_{jk}^2/(2m)$. The Hamiltonian for this mode then reduces to

$$H_{jk} = L \left(g\delta n_{jk}^2/2 + n\hbar^2k^2\theta_{jk}^2/(2m) \right). \quad (32)$$

This hamiltonian could also have been derived from the equations of motion given in Eq. (31), provided that the quantum pressure term $\hbar^2/(2m)\Delta\delta n/n$ is neglected: indeed, for a given wave vector k , the laplacians in Eq. (31) give a factor k^2 and Eqs. (31) are simply the equations of motion derived from the Hamiltonian Eq. (32). For temperatures much larger than ng , the thermal population of these phonon modes is large and classical statistics apply. Thus, the mean energy per quadratic degree of freedom is $T/2$ and we obtain

$$\langle \delta n_{jk}^2 \rangle = T/(Lg). \quad (33)$$

and

$$\langle \theta_{jk}^2 \rangle = mT/(Lnk^2\hbar^2). \quad (34)$$

We can now check the validity of the assumption $\delta n_k/n \ll \theta_k$: it is valid as long as $k \ll \sqrt{mgn}/\hbar$. Since k values are spaced by $2\pi/L$, there are about $L\sqrt{mgn}/(\pi\hbar)$ modes that satisfy this condition. Since the contribution of each of these modes to the relative density fluctuations is given in Eq. (33), we find that the contribution of these low momentum excitations to the relative density fluctuations is of the order of

$$\frac{\langle \delta n^2 \rangle_{\text{phonons}}}{n^2} \simeq \frac{T}{n\hbar\sqrt{gn}/m} \simeq \frac{T}{T_d\sqrt{\gamma}} \simeq T/T_{co} \quad (35)$$

For wave vectors much larger than \sqrt{mgn}/\hbar , the phase-density representation is not the most appropriate. An excitation of wave vector $k \gg \sqrt{mgn}/\hbar$ corresponds to the presence of an atom of momentum k , whose wave function is e^{ikz}/\sqrt{L} and whose energy is $\hbar^2 k^2/(2m)$. The annihilation operator for this mode is a_k as introduced in section 2.2. For temperatures much larger than $\hbar^2 k^2/m$, the thermal population of this mode is large and classical field theory, in which a_k is treated as a c-number, is adequate. We then find that a_k has a Gaussian distribution which satisfies $\langle |a_k|^2 \rangle = 2mT/(\hbar^2 k^2)$. The density fluctuations caused by the presence of such high momentum atoms result mainly from the interference between the atomic field $a_k e^{ikz}/\sqrt{L}$ and the atomic field of long wavelength spatial variations, whose amplitude is close to \sqrt{n} . The density fluctuations are thus $\delta n = \sqrt{n}(a_k e^{ikz} + a_k^* e^{-ikz})/\sqrt{L}$. We then find that the contribution of the mode of wave vector k to density fluctuations is $\delta n_k^2 = 4nmT/(L\hbar^2 k^2)$. Summing the contributions of the modes for all $k > \sqrt{mgn}/\hbar$, we obtain an estimate of the density fluctuations $\langle \delta n^2 \rangle_{\text{atoms}}$ caused by high momentum excitations:

$$\frac{\langle \delta n^2 \rangle_{\text{atoms}}}{n^2} \simeq \frac{T}{T_d\sqrt{\gamma}} \simeq \frac{T}{T_{co}}. \quad (36)$$

One also sees from the above argument that the density fluctuations fall off as $1/k^2$ above $k = \sqrt{mgn}/\hbar$. The inverse of this scale gives the length scale of density fluctuations and we find that this correlation length is the healing length ξ defined in Eq. (28).

From Eq. (35) and Eq. (36), we find that $\delta n^2/n^2 \simeq T/T_{co}$. Thus, the quasi-condensate treatment is valid as long as $T \ll T_{co}$. In conclusion, we have shown that T_{co} gives the limit of both the ideal gas regime, valid as long as $T \gg T_{co}$, and the limit of the quasi-condensate regime, valid for $T \ll T_{co}$. Equivalently, in terms of chemical potential, as long as the chemical potential is positive and much larger than μ_{co} of Eq. (26), the gas is in the quasi-condensate regime whereas for negative chemical potential of absolute value much larger than μ_{co} the gas is in the ideal gas regime. This is illustrated in Fig. 3. The two regimes differ by the fact that the $g^{(2)}(z)$ function is modified: it is close to one for any z in the quasi-condensate regime while $g^{(2)}(0) = 2$ in the ideal gas regime.

2.3.2 Phase fluctuations

In the quasi-condensate regime, although the gas is coherent with respect to the $g^{(2)}$ function, it is not coherent with respect to the $g^{(1)}$ function. This is why the gas is called a *quasi*-condensate. The phase fluctuations have been measured experimentally in various experiments where the

quasi-condensate presented a one-dimensional character [34, 35, 36, 37, 38]. The description of the quasi-condensate given above permits a simple calculation of those phase fluctuations as we now show. Phase fluctuations are given by

$$\langle (\theta(z) - \theta(0))^2 \rangle = \sum_{k>0} 2\langle \theta_{ck}^2 \rangle (\cos(kz) - 1)^2 + \sum_{k>0} 2\langle \theta_{sk}^2 \rangle \sin^2(kz). \quad (37)$$

Using Eq. (34) and $(\cos(kz) - 1)^2 + \sin^2(kz) = 2(1 - \cos(kz))$ this gives

$$\langle (\theta(z) - \theta(0))^2 \rangle = 4(mT/(Ln\hbar^2)) \sum_{k>0} \frac{1 - \cos(kz)}{k^2}. \quad (38)$$

Transforming \sum_k into $L/(2\pi) \int_0^\infty dk$ and using $\int_0^\infty (1 - \cos(kz))/k^2 dk = \pi z/2$, we obtain

$$\langle (\theta(z) - \theta(0))^2 \rangle = \frac{mTz}{n\hbar^2} = \frac{2\pi z}{n\lambda_{dB}^2}. \quad (39)$$

Since density fluctuations are very small, the $g^{(1)}$ function is about $g^{(1)}(z) = n\langle e^{i(\theta(z) - \theta(0))} \rangle$. Since the Hamiltonian is quadratic, we can use the Wick theorem to compute $\langle e^{i(\theta(z) - \theta(0))} \rangle$, which gives $\langle e^{i(\theta(z) - \theta(0))} \rangle = e^{-\langle (\theta(z) - \theta(0))^2 \rangle / 2}$. We find

$$g^{(1)}(z) \simeq e^{-mTz/(2n\hbar^2)}. \quad (40)$$

Comparing this to Eq. (18), we observe that the behavior of $g^{(1)}$ is close to that in the ideal gas regime. The factor of 2 difference in the correlation length formulae is because for the ideal gas regime, both density and phase fluctuations contribute to $g^{(1)}$ whereas only phase fluctuations remain in the quasi-condensate regime. The crossover from the ideal gas regime to the quasi-condensate regime, at a temperature T_{co} , Eq. (25), corresponds to the situation where the correlation length of phase fluctuations, given by Eq. (40), equals the correlation length of density fluctuations given by Eq. (28).

In both this section and the previous one, we assumed that the temperature is high enough that the population of the relevant modes (whose wavelengths are of the order of ξ) is much greater than unity. This is no longer the case when T reaches values of the order or smaller than gn . For lower temperatures, quantum fluctuations are expected to be dominant. This is the so-called quantum quasi-condensate and the boundary between the thermal quasi-condensate regime and the quantum quasi-condensate regime is at $T \approx ng$, corresponding to

$$t \approx \frac{1}{\gamma} \quad (41)$$

and is shown as a line in Fig. 1. A recent experiment using an atom chip observed these quantum phase fluctuations [39]. In the experiments we describe here however, the temperature is high enough that thermal fluctuations dominate.

2.4 Exact thermodynamics

In sections 2.2 and 2.3, we have discussed models that apply independently in the asymptotic limits of the nearly ideal gas regime ($T \gg T_{co}$ or equivalently $-\mu \gg \mu_{co}$) and the quasi-condensate regime ($T \ll T_{co}$ or equivalently $\mu \gg \mu_{co}$) respectively. While the above classification gives very useful insight, it should be emphasized that the boundary between these two regimes is a smooth crossover, not a sharp transition and that neither of the two theories presented above account for the physics in the vicinity of the crossover. Since in many cases we are interested in the precise behavior near the crossover from the ideal gas to the quasi-condensate regime, it is not sufficient to use the asymptotic results.

As already mentioned in the introduction, the 1D Bose gas with repulsive delta-function interactions is an example of an exactly solvable model [40, 41]. This allows us to quantitatively compare predictions of the two approximate descriptions to the exact results, and verify the regions of validity of the approximations. Furthermore the exact results will turn out to be important for an accurate description of the experiments.

Exactly solvable models typically occur in lower dimensions (1D quantum systems [40, 41] and 2D classical systems [42]) and allow one to obtain exact solutions for the quantum many-body eigenstates through a method known as the “Bethe Ansatz” (due to Hans Bethe [43]), for *any* value of the interaction strength. For the repulsive delta-interacting 1D Bose gas (with periodic boundary conditions), these solutions were first obtained by Eliot Lieb and Werner Liniger [10, 11]. Furthermore, the method based on the Bethe Ansatz can be extended to also obtain the thermodynamics exactly (for *any* temperature), via a method due to C. N. Yang and C. P. Yang [12].

For a concise and lucid description of the Yang-Yang method to obtain the exact thermodynamics of the 1D Bose gas and the related equations, we refer the reader to the original literature [12]. In brief, each exact quantum many-body eigenstate of the Lieb-Liniger hamiltonian Eq. (1) is characterized by a set of distinct integer quantum numbers and a corresponding set of distinct quasi-momenta k , obtained through the Bethe Ansatz. For a large system, one can consider the distribution of these quasi-momenta $\rho(k)$ and also of the “holes” $\rho_h(k)$, the latter corresponding to the “missing” values in the set of integers characterizing the individual quantum states. By considering the entropy for given distributions $\rho(k)$ and $\rho_h(k)$, Yang and Yang showed that the condition of thermal equilibrium leads to a set of nonlinear integral equations that can be solved by iteration. Subsequently, from the resulting distributions thermodynamic quantities such as pressure and free energy can be obtained. Once these quantities have been found, further thermodynamic quantities can be calculated using the standard thermodynamic relations.

Although numerical solutions to the Yang-Yang equations were already obtained at an early stage by C. P. Yang [44], important further insight into the Yang-Yang thermodynamics was gained much more recently by Kheruntsyan, Gangardt, Drummond and Shlyapnikov [22, 23]. They calculated both density and the normalized local density-density correlation function $g^{(2)}(0)$, and compared to approximate results in the various regimes discussed above. The former, $n(\mu, T)$, is obtained as part of the equation of state. The latter is obtained from the derivative of free energy with respect to the coupling constant g , using the Hellmann-Feynman theorem.

As an important example, a comparison to the approximate results of the previous sections

is shown in Fig. 3, for a fixed scaled temperature of $t = 1000$. This value is in the relevant range for the experiments to be described below. Such curves as a function of chemical potential μ are particularly useful to describe the behavior in a trap, since in this case one has a well-defined global temperature, while the density varies (within the local density approximation) with the local chemical potential $\mu(z)$ according to $\mu(z) = \mu - V(z)$, where $V(z)$ is the trapping potential. This will be discussed in more detail in the following section.

Figure 3(a) shows that the exact density ($n \propto 1/\gamma$) indeed approaches the ideal-gas behavior as μ/μ_{co} becomes sufficiently negative, while for large positive μ/μ_{co} it approaches the quasi-condensate result. There is a large range in density (more than a factor 4) over which neither asymptotic description gives correct predictions. In the same vein, the local density-density correlation function $g^{(2)}(0)$ (Fig. 3(b)) smoothly crosses over from 2, the value for an ideal gas, to about 1, as expected for a quasi-condensate. This smoothness is characteristic of crossover behavior, and is drastically different from the step-like behavior typical for a 3D gas.

Looking more closely at Fig. 3, one sees that the ideal gas description begins to fail for a gas that is only moderately degenerate: already at $\mu/T = -0.5$ ($\mu/\mu_{co} = -5$ for the considered t parameter), a chemical potential for which $n\lambda_{dB} \approx 10$ and the population in the $k = 0$ mode according to Eq. (12) is ≈ 1.5 , the ideal Bose gas prediction is off by about 10%. This is because the interaction-induced crossover is sufficiently wide that for the used value of t (1000), the chemical potential at degeneracy ($\mu/T \approx -1$) is not very far removed. The narrowness of the degenerate ideal gas regime is also seen in Fig. 1. To achieve well separated regimes, one would need to work at much higher t and much smaller γ . For $t = 1000$, the effect of degeneracy is nevertheless visible before the quasi-condensate crossover. This is shown by comparing the density with both the true ideal gas model and the Maxwell-Boltzmann model in Fig. 3: at $\mu/\mu_{co} \simeq -5$ the ideal gas model gives a prediction for the density accurate within 10% as mentioned above (and the nearly-ideal-gas description can thus be expected to be applicable) while the Maxwell-Boltzmann prediction is off by a factor of about 2.

Concerning the local pair correlation function $g^{(2)}(0)$, it deviates from the ideal-gas value of 2 for the entire range plotted in the figure. The experiments presented in this chapter however (see Sec. 4), are not precise enough to detect this deviation. Finally, the value of $g^{(2)}(0)$ can take values below unity in the quasi-condensate regime. We will briefly return to this point in Sec. 4.3.3.

Despite its power, the Yang-Yang theory does not permit calculation of any non-thermodynamic quantities. For example, only the *local* value of the density correlation function $g^{(2)}(0)$ has been obtained from thermodynamics, while the full behavior of $g^{(2)}(z)$ has been obtained from the exact solution only at zero temperature [46]. At finite temperature, the behavior of $g^{(2)}(z)$ has been obtained only by perturbative calculations valid in each asymptotic regime [47], but they do not describe the crossover itself. An alternative approach uses the fact that the crossover appears in a highly degenerate gas. In this case, the modes are highly populated and a classical field approach is possible [48, 49].

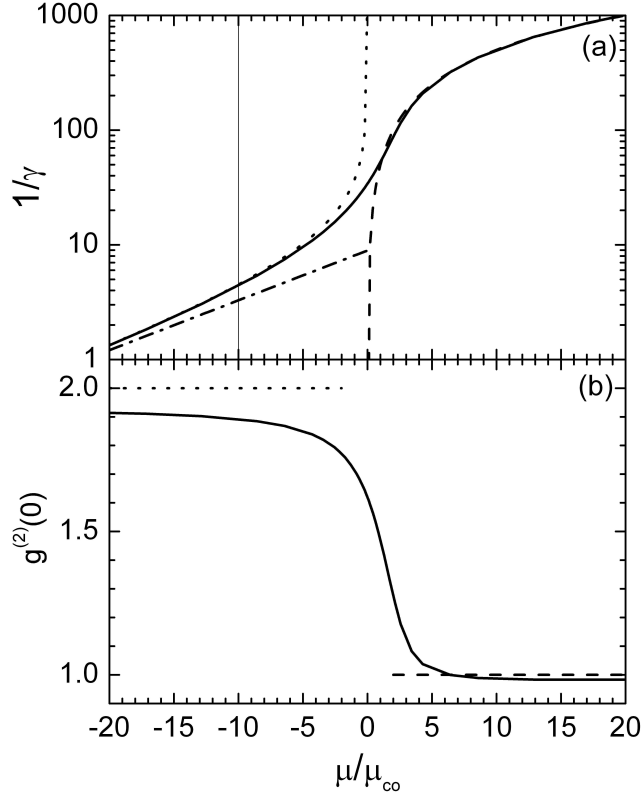


Figure 3: Normalised density ($1/\gamma$) and local pair correlation $g^{(2)}(0)$ as a function of chemical potential scaled to the crossover chemical potential μ_{co} given in Eq. (26) for fixed temperature corresponding to $t = 1000$. Numerical results from the Yang-Yang equations (solid lines, courtesy K. Kheruntsyan) are compared to the ideal Bose gas model (dotted line in (a), Eq. (13)) and the quasi-condensate model (dashed line in (a), Eq. (30)). The vertical line in (a) indicates the degeneracy chemical potential $-\mu = T$. The classical Maxwell-Boltzmann prediction Eq. (15) is shown as dashed-dotted line. In (b) the asymptotic values of $g^{(2)}(0)$ are indicated for both the ideal-gas regime ($g^{(2)}(0) = 2$ for $\mu \ll -\mu_{co}$, dotted line), and the quasi-condensate regime ($g^{(2)}(0) = 1$ for $\mu \gg \mu_{co}$, dashed line). Adapted from Refs. [45, 38].

3 1D gases in the real world

In real experimental situations, the atomic gas is neither homogeneous nor purely one-dimensional. As usual, in our experiments the trapping is to a good approximation harmonic. The trap has cylindrical symmetry and is characterized by a tight radial trapping frequency ω_{\perp} and a much lower axial trapping frequency ω . Here, we briefly summarize the main issues related to realizing a 1D system in this trapping geometry. We first discuss the link between transverse effects related to ω_{\perp} and we present a model based on the Yang-Yang thermodynamics, valid at low enough linear densities, that takes into account these transverse degrees of freedom. We then discuss the effect of the longitudinal trapping potential. We finish by discussing the link with the 3D physics, in particular with regard to the usual Bose-Einstein condensation in 3D.

3.1 Transverse trapping and nearly 1D Bose gases

Strictly speaking the conditions to be 1D in a transversely trapped gas are that both temperature and chemical potential are much smaller than the radial vibration quantum, $T, \mu \ll \hbar\omega_{\perp}$. If this is the case, the gas is frozen in the transverse direction both thermally and in terms of chemical potential, and the (many-body) wave functions can be factorized into the product of a transverse part (the gaussian ground-state wavefunction of the radial trap) and an axial part. The system is then kinematically one-dimensional. Studying the scattering properties, Ref. [20] has shown that the interactions can be modeled by an effective 1D coupling constant g and, as long as the 3D scattering length a is much smaller than the typical size of the transverse oscillator wavefunction, $l_{\perp} = \sqrt{\hbar/m\omega_{\perp}}$,

$$g = 2a\hbar\omega_{\perp}. \quad (42)$$

In most experiments on atom chips, neither of the above conditions on temperature and chemical potential are well-fulfilled, and it is necessary to also take into account the transverse degrees of freedom.

It is useful to consider the linear density n_l , obtained from the actual 3D density $\rho(x, y, z)$ through integration

$$n_l(z) = \int \int dx dy \rho(x, y, z). \quad (43)$$

When the gas is strictly 1D, one can identify n_l with the 1D density n . We will present our main experimental results in terms of this linear density, because it turns out that n_l is often the key parameter, in particular when considering the crossover to 3D at low temperatures.

This is in particular true for the quasi-condensate regime, at temperatures $T \ll \hbar\omega_{\perp}$. In this regime, the chemical potential is close to its value at zero temperature, which is given by the solution of the radial Gross-Pitaevskii equation [50, 51]. It was found from comparison to numerical integration of the radial Gross-Pitaevskii equation [50, 51] that, in the quasi-condensate

regime, to good approximation the chemical potential can be expressed as²

$$\mu = \hbar\omega_{\perp} (\sqrt{1 + 4n_l a} - 1). \quad (44)$$

For linear density $n_l \ll 1/4a$, we find that $\mu \simeq 2\hbar\omega_{\perp} a n_l$. We recover here the chemical potential gn of the 1D case. At larger linear density, the chemical potential is reduced compared to the formula $2\hbar\omega_{\perp} a n_l$. This reflects the fact that, for large densities, the transverse cloud size is increased with respect to the transverse vibrational ground state. As another example of how n_l is the relevant quantity for low enough temperatures, we note that the expression Eq. (40) for the phase coherence length remains correct also on the 3D side of the crossover, if we replace the 1D density n by the linear density n_l [52].

3.2 Applying 1D thermodynamics to a 3D trapped gas

Another case that one can consider is when the interaction energy is in the 1D regime, $ng \ll \hbar\omega_{\perp}$, while temperature is in the 1D-3D crossover, $T \simeq \hbar\omega_{\perp}$. A model for this regime was introduced in Ref. [8], and we describe it here. The key step is to separately consider the radial states. Under the above conditions only the radial ground state is significantly affected by the interactions, while the radially excited states can still be treated as an ideal gas. Thus, for the radial ground state, the solution $n_{YY}(\mu, T)$ to the Yang-Yang equations must be used. Each radially excited state with radial quantum number $j \geq 1$ is now considered as an independent ideal 1D gas, in thermal equilibrium with the rest of the cloud. Each of the radially excited states is thus taken to have a density (cf. Eq. (13))

$$n_e(\mu_j, T) = \frac{1}{\lambda_{dB}} g_{1/2}(\exp(\mu_j/T)), \quad (45)$$

where an effective chemical potential μ_j has been introduced that takes into account the radial excitation energy,

$$\mu_j = \mu - j\hbar\omega_{\perp}. \quad (46)$$

Taking into account the degeneracy factor $j + 1$ of the radially excited states, the total linear density in this model thus becomes

$$n_l(\mu, T) = n_{YY}(\mu, T) + \sum_{j=1}^{\infty} (j + 1) n_e(\mu_j, T). \quad (47)$$

As long as $\mu < \hbar\omega_{\perp}$, we have $\mu_j < 0$ which is necessary to avoid divergence of $g_{1/2}$ in Eq. (45). In fact, from the previous discussion in Sec. 2.4, for our parameters ($t \approx 1000$), we can expect an ideal-gas treatment of the radially excited density to begin to break down for $\mu_j/T > -0.5$ since this is where interactions will become important. In practical cases where $T \approx \hbar\omega_{\perp}$, the model should thus be accurate as long as $\mu < 0.5\hbar\omega_{\perp}$, while for $\mu > 0.5\hbar\omega_{\perp}$ the model will start to become inaccurate.

²An additional factor -1 has been introduced in brackets in Eq. (44) compared to Ref. [51]. This subtracts the radial zero-point energy $\hbar\omega_{\perp}$, so that $\mu = 0$ corresponds to the energy of the lowest energy ($k = 0$) state, as in the treatment in Sec. 2.

3.3 Longitudinal trapping

Experimentally, cold gases are axially confined in a confining potential $V(z)$ and the cloud is not infinite and homogeneous as assumed in the previous section. However, as seen below, for weak enough axial confinement, the results for homogeneous gases can be applied using a local density approximation. In the first following sub-section, we present the local density approximation and discuss its predictions. We then evaluate the condition of validity of this approximation.

3.3.1 Local density approximation

If the confinement is weak enough that the correlation length of the gas is, at each position, much smaller than the length of the mean density variations, then the gas may be divided into small slices in which the thermodynamics of uniform systems applies. A slice located at position z is in equilibrium with the rest of the gas. It is thus described by the grand canonical ensemble at temperature T and at a chemical potential μ_0 . The energy of the gas contained in this slice is shifted by the quantity $V(z)$. It is equivalent to assuming that the chemical potential is $\mu_0 - V(z)$, while the energy of the gas is unshifted. Thus, the local properties of the gas are that of a homogeneous infinite gas at temperature T and local chemical potential $\mu(z) = \mu_0 - V(z)$. This is the so-called local density approximation.

Within the local density approximation, all the results presented in the previous section hold. Thus, performing local analysis, one can observe all the features of homogeneous 1D gases: the presence of the ideal gas regime, which includes the degenerate regime, the crossover towards a quasi-condensate and the quasi-condensate regime. In particular, a quasi-condensate appears in the center of the trap, when the peak density exceeds the crossover density n_{co} given by Eq. (24).

It is often interesting to investigate the behavior of the gas using the extensive variable N , where N is the total atom number. As long as the peak density is much smaller than n_{co} , the density profile is well described using the equation of state $n(\mu, T)$ of an ideal Bose gas. Then the total atom number is easily computed and, for gases that are degenerate at the trap center, we obtain [45]

$$N = T/(\hbar\omega) \ln(T/|\mu_0|). \quad (48)$$

The atom number at the crossover towards a quasi-condensate is obtained when the peak density reaches n_{co} . Inserting Eq. (16) and Eq. (24) into Eq. (48) we find that the atom number at the crossover is approximately

$$N_{co} = T/(\hbar\omega) \ln((\hbar^2 T/(mg^2))^{1/3}) = T/(3\hbar\omega) \ln(t/2). \quad (49)$$

Since $t^{1/3} \gg 1$ (see text below Eq. (24)), this equation can be inverted to give a crossover temperature

$$T_{co} = N\hbar\omega / \ln((N\hbar^3\omega/(mg^2))^{1/3}). \quad (50)$$

A comparison of this formula with a numerical calculation using Yang-Yang thermodynamics shows very good agreement [45]. Since $t \gg 1$ at the crossover, Eq. (49) shows that the ratio N_{co}/N_d , where $N_d = \hbar\omega/T$ is the atom number at degeneracy, is larger than one at the crossover. Thus, even considering the extensive variable N , the degenerate ideal gas regime is in principle

identifiable. However, the ratio N_{co}/N_d only grows as logarithm of t and it is in practice difficult to have N_{co}/N_d very large.

3.3.2 Validity of the local density approximation

All the previous results use the local density approximation, which requires that the correlation length l_c of the gas be much smaller than the scale L of variation of the density. At the crossover, the correlation length of the gas is about $l_c \simeq \xi = \hbar/\sqrt{mgn}$, as seen in section 2. To estimate L , let us approach the crossover from the ideal gas regime. The density profile of the central part of the cloud, obtained using Eq. (16) and the local chemical potential $\mu(z) = \mu_0 - m\omega^2 z^2/2$, turns out to be a lorentzian of width $\sqrt{|\mu_0|/m\omega^2}$. Thus, $L \simeq \sqrt{|\mu_0|/m\omega^2} \simeq (gT_{co}/m\hbar\omega^3)^{1/3}$ at the crossover. We thus find that the condition of validity of the local density approximation, $l_c \ll L$, can be rewritten as

$$\omega \ll \omega_{co} = \frac{(E_g T^2)^{1/3}}{\hbar} = \frac{\mu_{co}}{\hbar}, \quad (51)$$

a result which has been derived in [45].

If the local density approximation (51) is not satisfied, the discrete structure of the trap energy levels has to be taken into account. In the opposite limit, $\omega \gg \omega_{co}$, the quantization of energy levels plays a role while the gas is still described by an ideal Bose gas. Then, it has been shown in [53] that one expects a condensation phenomenon to occur at a temperature

$$T_C = N\hbar\omega / \ln(2N). \quad (52)$$

In contrast to the crossover described in the previous section (referred to now as the interaction-induced crossover), this is a finite size phenomenon since T goes to zero when the trap confinement ω goes to 0, $N\omega$ being fixed. This condensation phenomenon will dominate the interaction induced crossover when $T_C > T_{co}$. This condition is equivalent to $\omega \gg \omega_{co}$, which shows consistency of our analysis.

Experimentally, the condition (51) to observe the interaction induced crossover is very easily satisfied: using Eq. (42), the condition (51) reduces to

$$\omega \ll \omega_{\perp} (T/\hbar\omega_{\perp})^{2/3} (a/l_{\perp})^{2/3}. \quad (53)$$

One can check that, for most alkali atoms, in trapping potentials with ω_{\perp} ranging from 1 to several tens of kilohertz and for temperatures between $0.1\hbar\omega_{\perp}$ and $\hbar\omega_{\perp}$, this condition is easily fulfilled, unless a is extremely small ($a < 0.1$ nm). Thus, one expects that a trapped 1D gas undergoes the interaction induced crossover towards a quasi-condensate and that the local density approximation is valid to describe the gas.

3.4 3D physics versus 1D physics

Experimentally, one expect a crossover from a one-dimensional behavior to a three dimensional behavior as the temperature of the gas increases and, at large enough temperature, one expects to recover the physics of a three-dimensional gas. The physics of a 3D gas is very different from

that of a 1D gas. The most striking difference is that, even in the absence of interactions, a 3D Bose gas undergoes a phase transition towards a BEC due to saturation of the population of the excited states. This is in contrast to 1D gases where, in absence of interactions between atoms, the gas behaves, for any density, as a thermal gas in which bosonic bunching is present. For weakly interacting gases, in both 1D and 3D gases, a transition towards a (quasi-)condensate is expected. However, these transitions are different in nature and this difference can be captured by studying the validity of mean field theories in both cases.

In 3D weakly interacting gases ($\rho a^3 \ll 1$), the effect of interactions between atoms on the onset of Bose Einstein condensation is very small. This is why 3D Bose gases with weak interactions are well described by mean field theories. For instance, the thermodynamics is given with a very good approximation by the Hartree-Fock-Bogoliubov self consistent theory [54,55]. In such a theory, at temperatures larger than the critical condensation temperature, the gas is described by the Hartree-Fock approach, in which correlations between atoms introduced by interactions are neglected. Condensation is then due, as for an ideal Bose gas, when the density reaches $2.612\dots/\lambda_{dB}$. For higher densities, a non zero condensate wave function appears, which is the order parameter of this second-order phase transition. The experimental value of the critical temperature in weakly interacting ultra-cold Bose gases is in good agreement with this theory [56].

However, even for weakly interacting gases, such a mean field theory is expected to fail very close to the critical point of temperature T_c . This is due to the large long wave length fluctuations that develop in the vicinity of the transition. In the condensate side, *i.e.* for $T < T_c$, the Hartree-Fock-Bogoliubov self consistent theory is valid only if the fluctuations of the condensate wave function, averaged over a volume of the order of the correlation length, are smaller than its mean-field value. This is the so-called Ginzburg criteria and it gives [55]

$$\frac{T_c - T}{T_c} \gg a\rho^{1/3}. \quad (54)$$

The same criterion (up to an absolute value) is true above T_c . The region around the transition where $|T_c - T|/T_c$ is of the order or smaller than $a\rho^{1/3}$ is not expected to be described by a mean-field. Beyond mean-field effect include a modification of the transition temperature. Since interactions tend to decrease long wave length density fluctuations, they favor the appearance of a condensate and, for small parameter $a\rho^{1/3}$, an increase of the critical temperature is expected [57, 58,59]. Such a modification is very small in cold atom experiments and has never been observed. A second non mean-field effect is the modification of the critical exponent that describes the divergence of the correlation length in the vicinity of the critical point. Measuring beatnodes between the atomic field extracted at different places in the atomic cloud, the critical exponent was measured recently in dilute atomic gases, in agreement with beyond mean-field theories [60].

The physics is very different in 1D systems, since long wavelength fluctuations play an enhanced role compared to 3D systems. The crossover towards a quasi-condensate is, in 1D gases, a phenomenon driven by interactions. More precisely, the crossover towards a quasi-condensate is produced by the correlations between atoms brought by the interactions. It cannot be captured by the Hartree-Fock theory because Hartree-Fock theory neglects correlations between atoms introduced by interactions. Thus, in real systems the failure of the Hartree-Fock theory to describe

the appearance of a (quasi-)condensate is a signature of the 1D nature of the physics involved.

4 Experiments

In this section we will discuss several experiments that have been carried out in both Orsay and Amsterdam using atom chips which probe the ideas discussed in the previous sections. Atom chip setups are very well suited to study one-dimensional geometry since very tight atom guides are easily realised by going close to a current-carrying micro-wire. The atom chips which were used in the experiment presented below are sufficiently similar that we will attempt to describe both at once. We will refer the reader to the individual experiments for more detailed information. The atom chips we used employed current carrying wires to create magnetic trapping fields for ^{87}Rb atoms in the $F = 2, m_F = 2$ state. Magneto-optical traps, laser cooling and evaporative cooling were used to load atoms into the chip-based traps, which tended to be highly confining but rather shallow. Typical currents were on the order of a few amperes and the atoms were at a distance of several tens of microns from the wire surface. Typical transverse confinement frequencies ($\omega_{\perp}/2\pi$) were about 3 kHz, while longitudinal frequencies were on the order of 10 Hz. This transverse frequency corresponds to a temperature $\hbar\omega_{\perp}/k_B$ of 144 nK, and evaporative cooling was able to reach a temperature equal to or slightly above this value. For Rb atoms, with 3D scattering length $a = 5.24$ nm, the energy scale E_g corresponds to 0.20 nK, and 144 nK in reduced temperature units corresponds to $t = 720$. Since the longitudinal trapping potential is roughly harmonic, the linear atom density varied in space, and thus a single sample permits one to probe a large range in density at constant temperature. A single density profile thus corresponded to a horizontal line in Fig. 1. The value of the parameter γ was typically between 10^{-1} to 10^{-3} . The data consisted of absorption images of the cloud, taken either *in situ* or after a very short expansion time. Temperature measurements were made by fitting the wings of the cloud, or by fitting to the Yang-Yang model (see description below).

The first set of measurements we describe are simple observations of the density profiles of nearly one-dimensional gases on an atom chip. The measurements were carried out with two purposes in mind. In the first measurements, carried out in Orsay, emphasis was placed on proving that in the region of the crossover between the ideal gas and quasi-condensate regimes, no theoretical approach which neglected interaction induced correlations between particles, in particular the Hartree-Fock approach, could explain the profiles. In the second set, carried out in Amsterdam, it was shown that the exact thermodynamic treatment accounted very well for the entire observed profile, notably when the gas was in the crossover regime. After examining the profiles we move to another type of measurement in which the absorption images were analyzed to give information about density fluctuations. Although these measurements were chronologically the first, we will treat them last.

4.1 Failure of the Hartree-Fock model

A typical density profile is shown in Fig. 4. Superimposed on the data are three different theoretical predictions. The dashed line shows the profile as predicted by the ideal gas model. In the

wings of the profile this model should be valid, and indeed the fit to the wings of the distribution was used to deduce the temperature and the chemical potential of the gas. Clearly, however the ideal gas prediction begins to rapidly deviate from the data, because, without interactions, a 1D Bose gas can accommodate arbitrarily high densities at a given temperature. The dash-dotted line shows the prediction of the quasi-condensate model Eq. (44), at the same chemical potential as was found by fitting the wings. This model accurately reproduces the high density part of the distribution, but not the presence of so many atoms in the wings of the distribution.

The Hartree-Fock theory is a variational method in which the atoms are described by a gas of non interacting bosons subject to an effective potential V_{HF} due to the mean field of the other atoms. Minimizing the free-energy of the gas, one finds

$$V_{HF}(\mathbf{r}) = 2g_{3D}\rho \quad (55)$$

where $g_{3D} = 4\pi\hbar^2 a/m$ is the 3D coupling constant and ρ is the 3D gas density. This theory is thus self consistent, since for a given chemical potential and temperature, ρ depends on V_{HF} . The factor 2 reflects the bunching, which is present in the Hartree-Fock approximation since the gas is described by a gas of non interacting bosons.

Using minimisation techniques, the Hartree-Fock density profile was calculated in Ref. [6] for the experimental three-dimensional trapping potential and for the temperature and chemical potential found by fitting the wings of the distribution. One sees that the Hartree-Fock density profile, shown as a solid line in Fig. 4, reproduces the wings of the density profile, and does not diverge as does the ideal gas profile. It does not however, reproduce the high density part of the profile. Moreover, the Hartree-Fock calculation shows that the Hartree-Fock gas is far from being saturated: the population of the ground state is very small, and no condensation is expected according to this mean-field model. The excess of atoms in the center is the onset of a quasi-condensate, although the cloud is not deep into the quasi-condensate regime. This peak is formed by the effects of interactions altering the two body correlation function so as to lower the interaction energy relative to a Hartree-Fock gas at the same density.

4.2 Yang-Yang analysis

Two more examples of axial density profiles measured [8] at two different temperatures and a peak linear density of $\approx 50 \mu\text{m}^{-1}$ are shown in Fig. 5. These profiles were fit to the model based on the exact Yang-Yang solutions described in Sec. 3.2. The fits are shown in the Figure as continuous curves, and the resulting temperature T and chemical potential μ are also indicated. The chemical potential μ and the temperature T are the only free parameters in the model, and it was found that the full set of *in situ* measurements could be explained by the Yang-Yang-based model [8]. For comparison, The ideal-gas prediction and the quasi-condensate prediction are also shown. Clearly, the Yang-Yang-based model describes the entire profiles well, while the approximate models fail, in particular the smooth crossover between the two approximate models in the region where $\mu(z) \approx 0$ is captured very well by the model.

This analysis was further corroborated by measurements of the axial momentum distribution [8], obtained using Bose gas focusing [37]. The tails of the momentum distribution were used to

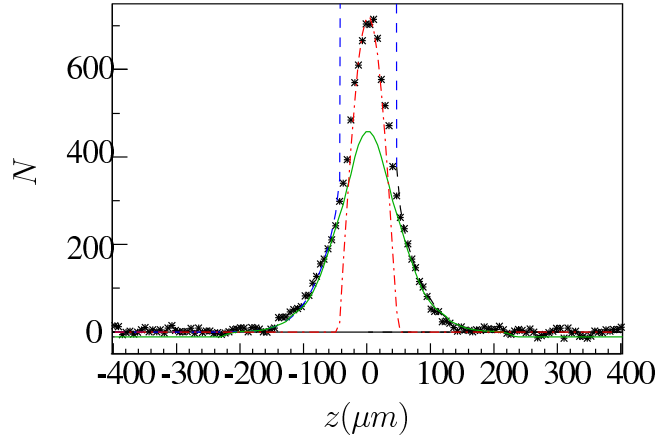


Figure 4: *Failure of Hartree-Fock theory in a quasi-1D gas. The experimental profile (crosses) is compared with the profiles expected for a quasi-condensate (dotted-dashed), for an ideal Bose gas (dashed), and to the profile predicted by the Hartree-Fock theory (continuous line) for the same temperature and chemical potential. The vertical axis is the number of detected atoms per $6 \mu\text{m}$ longitudinal pixel. The temperature of the gas was $T = 360 \text{ nK} = 2.75\hbar\omega_{\perp}$. Adapted from Ref. [6].*

extract temperatures, and these were found to agree very well with the temperatures derived from the Yang-Yang fit to the *in situ* data. The full momentum distribution is not a thermodynamic quantity, and can thus not be obtained directly from the Yang-Yang analysis.

The similarity of the measured density profiles of Figures 5(b) and 4 clearly suggests that the same physics of an interaction-induced crossover applies to both experiments. Although it is tempting to apply the Yang-Yang-based analysis of Sec. 3.2 also to the data of Fig. 4, this has not been done. It is likely that the result would not be quantitatively accurate, because at the higher linear densities and temperatures of Fig. 4, the validity limits of the model of Sec. 3.2 are reached near the peak of the profile (since both $\mu \approx \hbar\omega_{\perp}$ and $T \approx \hbar\omega_{\perp}$). Interactions are then expected to also play a role in the radially excited states, and also interactions among the different radial states will be significant.

4.3 Measurements of density fluctuations

As we have emphasized in Sec. 2, the transition towards a quasi-condensate in 1D gases is characterized by the inhibition of atom bunching, the large density fluctuations characteristic of a thermal Bose gas. A direct measurement of the density fluctuations through the crossover thus captures an essential characteristic of the crossover.

The measurement of density fluctuations proceeds similarly to the density profile measurements. The difference is that many (about 300) profiles are acquired and, roughly speaking, for each observation pixel, we compute the variance of the density measurements as well as the mean. We can relate this variance to the density fluctuations predicted by various theoretical approaches as described below.

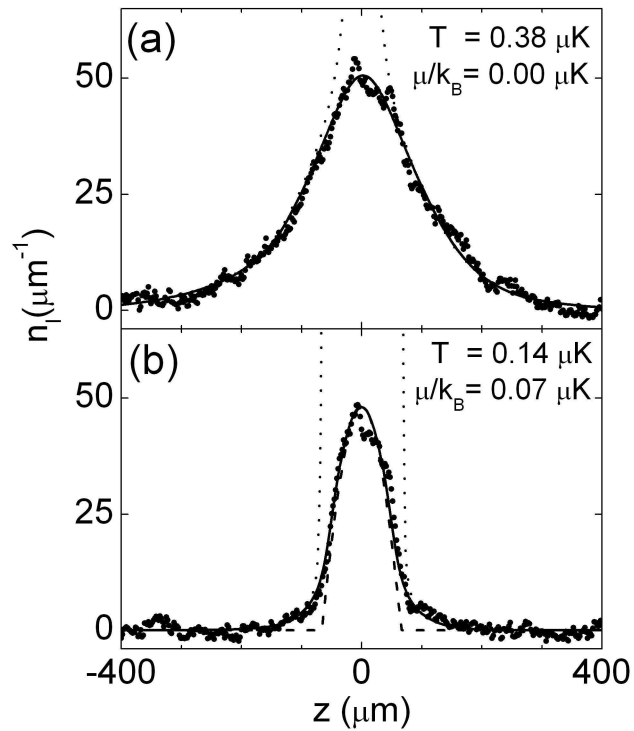


Figure 5: Comparison of experiment to Yang-Yang thermodynamics. The model described in Sec. 3.2 is fit to two examples of measured linear densities n_l (dots) in the Amsterdam experiment [8, 38]. The resulting fits (continuous curves) yield chemical potential μ and temperature T as indicated. Dotted curves: ideal-gas profile at the same temperature and chemical potential exhibiting divergence for $\mu(z) = 0$. Dashed curve in (b): quasi-condensate profile with the same peak density as the experimental data. In these experiments $\hbar\omega_{\perp} = 158$ nK. Adapted from Ref. [8].

The measurements involve several subtleties requiring careful normalizations and corrections of the data. These are described in detail in [7, 61]. The measurement requires a high degree of reproducibility in the data. The atom chip geometry permits the construction of a very compact apparatus with low sensitivity to vibration. The images contain not only noise due to atom fluctuations, but also photon shot noise. The photon noise must be carefully characterized and subtracted. Examples of the data are shown in Figs. 6 and 7.

4.3.1 A local density analysis

The pixel size in the experiment is $\Delta = 6 \mu\text{m}$. The pixel size is much larger than the correlation length of the gas which is always smaller than a micron in these experiments, but much smaller than the longitudinal length scale of mean density variation. Thus, the data should reproduce number fluctuations predicted in a longitudinal local density treatment. More precisely, the gas contained in the pixel located at position z can be described as a gas, confined transversely by the transverse potential of frequency ω_{\perp} and confined longitudinally by a box like potential of size Δ . The properties of this slice, which can exchange energy and particles with the rest of the gas, is well described within the grand-canonical ensemble. The energy shift $V(z)$ of this slice can be converted to a shift $-V(z)$ of the chemical potential. This is the local density approximation, already discussed in sec. 3. Since Δ is large compared to correlation length of the gas, the boundary conditions used to compute thermodynamic quantities are all equivalent and we use the periodic boundary conditions in the following.

Within the local density approximation, the confinement potential $V(z)$ is irrelevant to analyze the atom-number fluctuations. The atom number fluctuation δN^2 in each pixel depends only on the temperature T and on the local chemical potential. Equivalently, δN^2 is a function of T and $\langle N \rangle$, since the linear density is a monotonically increasing function of the chemical potential. We thus choose, for each cloud temperature, to represent the measured atom number fluctuation as a function of the mean atom number in the pixel. Experimental results are shown in Fig. 6 and fig. 7.

4.3.2 Ideal gas regime : observation of bunching

If the gas within a pixel can be considered ideal, we can use the results of Sec. 2.2. The fluctuations of atom number n_i in each one-atom quantum state $|i\rangle$ are

$$\langle n_i^2 \rangle - \langle n_i \rangle^2 = \langle n_i \rangle + \langle n_i \rangle^2. \quad (56)$$

The fluctuations of the total atom number N are thus

$$\langle N^2 \rangle - \langle N \rangle^2 = \langle N \rangle + \sum_i \langle n_i \rangle^2, \quad (57)$$

where the sum is performed over all the quantum states. The mean values $\langle n_i \rangle$ are given by the Bose distribution and the fluctuations of N are easily computed.

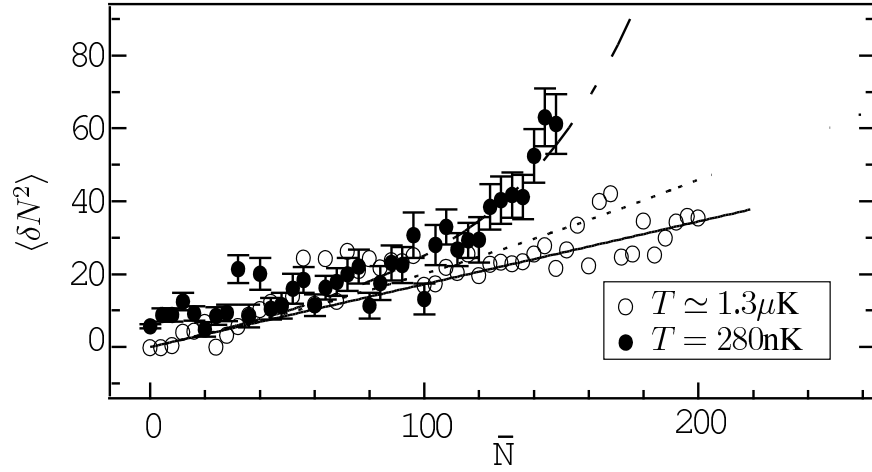


Figure 6: *Density fluctuations of a gas on an atom chip. The atom number variance in an observation pixel ($6 \mu\text{m}$) is plotted as a function of the mean number. The open circles are the fluctuations measured for a hot cloud ($T = 1.3 \mu\text{K}$ corresponds to $10\hbar\omega_{\perp}$) for which bunching is unobservable because of the large number of transverse states involved. The variance is due to atom shot noise. Full circles correspond to a colder cloud, at a temperature $T = 2.1\hbar\omega_{\perp}$. The increase in fluctuations is due to bunching. The theoretical prediction for an ideal Bose gas at the same temperature is given by the dashed curve. The prediction for a nondegenerate cloud, Eq. (61), is shown as the dotted curve. The degeneracy of the gas is evident. Adapted from Ref. [7].*

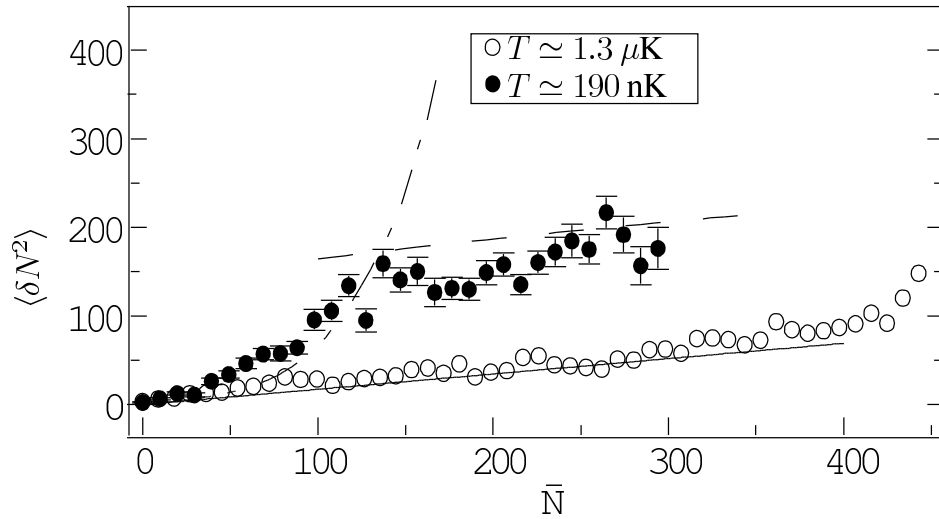


Figure 7: *Density fluctuations in the quasi-condensate regime. The dashed-dotted curve is the prediction for an ideal Bose gas at the same temperature as in figure 6. The dashed curve is the prediction for a quasi-condensate. In units of transverse energy, the temperature is $T = 1.4\hbar\omega_{\perp}$. Adapted from Ref. [7].*

A rough calculation is as follows: if M quantum states are populated with similar populations, Eq. (57) simplifies to

$$\langle N^2 \rangle - \langle N \rangle^2 = \langle N \rangle + \langle N \rangle \frac{\langle N \rangle}{M}. \quad (58)$$

The first term of the right hand side is the shot noise term, expected for uncorrelated, statistically independent atoms. The second term on the right hand side is the effect of the bunching. We see from this expression that as long as $\langle N \rangle/M$ is much smaller than 1, the bunching term is negligible compared to the shot noise term. The ratio $\langle N \rangle/M$ is approximately the phase space density of the gas and is much smaller than 1 if the gas is non degenerate. Thus one expects the measured atom number fluctuations to be dominated by the shot noise term for gases at high temperature. This is observed experimentally for non-degenerate clouds, as shown by the open circles in Fig. 6. The linearity of the measured value of $\langle N^2 \rangle - \langle N \rangle^2$ versus $\langle N \rangle$ shows that the fluctuations are given by the shot noise. The fact that the slope is smaller than the expected slope of 1 is due to the fact that the optical resolution (about 10 μm) is larger than the pixel size [7].

One can also give a more precise calculation of the fluctuations. For this purpose, we index the quantum states by the integer n_x and n_y , which label the transverse vibrational levels, and the longitudinal wave vector k_z , which takes values in multiples of $2\pi/\Delta$. For a highly nondegenerate gas, $|\mu| \gg T$, the population of each state is given by the Boltzmann law

$$\langle n_{n_x, n_y, k_z} \rangle = A e^{-(\hbar^2 k_z^2 / 2m + \hbar\omega_\perp (n_x + n_y)) / T}, \quad (59)$$

where the normalization factor A is

$$A = \frac{N \lambda_{dB}}{\Delta \sqrt{2\pi}} (1 - e^{-\hbar\omega_\perp / T})^2. \quad (60)$$

Inserting this into Eq. (57), we obtain

$$\langle N^2 \rangle - \langle N \rangle^2 = \langle N \rangle + \langle N \rangle^2 \frac{\lambda_{dB}}{\sqrt{2}\Delta} \tanh^2(\hbar\omega_\perp / 2T). \quad (61)$$

We thus recover an expression similar to Eq. (58), with $M = \sqrt{2}\Delta / (\lambda_{dB} \tanh^2(\hbar\omega_\perp / 2T))$. The \tanh term accounts for the number of populated transverse states. The term $\sqrt{2}\Delta / \lambda_{dB}$, which accounts for the longitudinal states, may be recovered by a semiclassical analysis: the volume of the occupied phase space is $\Omega \simeq \Delta \sqrt{mT}$ and the number of quantum states contained in this volume is of the order of Ω/\hbar . Equation (61) is valid if the gas is non degenerate. When the gas becomes degenerate, the distribution of the mean occupation number $\langle n \rangle$ versus the state energy becomes more peaked around zero. This amounts to a reduction of the effective number of occupied states M and the effect of bunching is larger than the prediction of Eq. (61). For highly degenerate gases, Eq. (61) underestimates the true fluctuations, which become large compared to the shot noise level.

The bunching effect is quite clear for a cold enough cloud as shown in Fig. 6. In this experiment, the bunching term is even larger than the shot noise term, indicating that the gas is

degenerate. The degeneracy is also shown by a comparison of the data with Eq. (61) shown as a dotted line. This equation, valid for a non degenerate gas, underestimates the measured fluctuations. On the other hand, a calculation of Eq. (57) using the true Bose occupation factor is in much better agreement with the data. This comparison shows that, at least as concerns fluctuations, the gas is well described by an ideal, degenerate Bose gas.

4.3.3 Quasi-condensate regime: saturation of atom number fluctuations

At sufficiently high density and low temperature, repulsive interactions between atoms are no longer negligible. As described in section 2, one expects the interactions to reduce the density fluctuations to lower the interaction energy. The gas then enters the quasi-condensate regime. For the temperature $T = 2.1 \hbar\omega_{\perp}$ of the data in Fig. 6, using Eq. (42) and assuming a purely 1D gas, Eq. (24) gives a density at the crossover of about 130 atoms per pixel. Although Eq. (24) does not apply since the gas is not purely 1D, this rough estimate shows that the crossover to a quasi-condensate is achievable at slightly higher atom number and/or lower temperature. Measurements of atom number fluctuations in a regime where the cloud center is in the quasi-condensate regime are shown in Fig. 7. Whereas at low atomic density the measured fluctuations are in agreement with the ideal Bose gas prediction, one sees a saturation of the fluctuations at higher densities.

To calculate the fluctuations, we first suppose the gas to be purely one dimensional, with a coupling constant g given by Eq. (42). In a local density approximation, we consider atom number fluctuations in a longitudinal box of length Δ in equilibrium with a reservoir of energy at temperature T and a reservoir of particles at chemical potential μ . As explained in sec. 2.3, the Hamiltonian is quadratic in δn in the quasi-condensate approximation and δn can be expanded as a sum of independent modes indexed by the wave vector k . The atom number fluctuations $N - \langle N \rangle$ are obtained by integrating δn over the pixel size. Thus, the only excitation that leads to atom number fluctuation is the zero momentum mode. Its energy, derived from Eq. (32), is

$$H_{k=0} = \Delta \frac{g}{2} \delta n_0^2. \quad (62)$$

Using the equipartition theorem, we find $\delta n_0^2 = T/(g\Delta)$. The atom number fluctuations, which are $(\Delta\delta n_0)^2$, are thus given by:

$$\langle N^2 \rangle - \langle N \rangle^2 = \frac{\Delta T}{g}. \quad (63)$$

Thus, we expect the atom number fluctuations to be independent of $\langle N \rangle$. The shot noise term is not present in this quasi-condensate regime: interactions between atoms prevent even the shot noise fluctuations and at temperature smaller than gn , one expects to observe sub-shotnoise fluctuations. This feature is also seen in Fig. 3 where $g^{(2)}(0)$ goes below unity in the exact solution.

In the experimental results shown in Fig. 7, the typical interaction energy is about $0.7\hbar\omega_{\perp}$. In these conditions, the transverse degrees of freedom cannot be neglected and the result of Eq. (63) must be corrected. More precisely, the phonons, which are longitudinal density waves, are associated with a breathing of the transverse shape of the cloud. For phonons of frequency much

smaller than the transverse frequency, the transverse shape of the cloud follows adiabatically the ground state equilibrium state for the local linear density. We denote by $E_{eq}(n)$ the energy of the gas per unit length for a linear density n . The phonon Hamiltonian of Eq. (32) is the term of the Hamiltonian of order two in δn and $\nabla\theta$. Thus, the interaction term of the phonons is $E_{\text{int}} = \frac{1}{2}L(\partial^2 E_{eq}/\partial n^2)\delta n_k^2$. Since $\partial E_{eq}/\partial n$ is the chemical potential of the gas (to zero order in δn), we can rewrite the former expression as $E_{\text{int}} = \frac{1}{2}L(\partial\mu/\partial n)\delta n_k^2$. In particular, the zero momentum term is

$$H_{k=0} = \frac{1}{2}L\frac{\partial\mu}{\partial n}\delta n_0^2. \quad (64)$$

Then, the atom number fluctuations are

$$\langle N^2 \rangle - \langle N \rangle^2 = \frac{\Delta T}{\partial\mu/\partial n}. \quad (65)$$

Although we derived this expression in the approximate quasi-condensate theory using expansion of the Hamiltonian to second order in δn , we recover here a well known result of statistical physics. More precisely, as shown in [62], Eq. (65) holds for any system in equilibrium with a particle reservoir at chemical potential μ and with an energy reservoir of temperature T .

To apply Eq. (65) to the experiment, we need the equation of state $\mu(n)$. Using Eq. (44) and Eq. (65), one can compute the expected fluctuations. Fig. 7 shows that the results are in fairly good agreement with the measured atom number fluctuations.

5 Conclusion

We hope that we have given the reader a useful overview of the physics of 1D gases in the weakly interacting regime. These systems are rich and manifest several different regimes separated by smooth crossovers. It is often necessary to appeal to many different physical models to understand them. The existence of exact solutions allows us to test the models and to explore their validity in the face of highly non-trivial many body correlations. Although the experimental and theoretical work we have described is quite extensive, we believe that much work remains to be done. The study of fluctuation phenomena is still at an early stage. For example the exact thermodynamics should admit a careful comparison with data such as that in Fig. 7, and improved experiments should probe larger parameter ranges and possibly even permit measurements of the correlation length. It may also be possible in the near future to enter the strongly interacting regime using an atom chip. Experiments are also capable of measuring momentum distributions [8], but so far no quantitative theoretical comparison has been made. Finally measurements of fluctuations and correlations in momentum space are also experimentally feasible [32].

6 Acknowledgments

We thank K. Kheruntsyan for a critical reading of the manuscript. NJvD acknowledges stimulating discussions with J.T.M. Walraven, G.V. Shlyapnikov, J.S. Caux, and A.H. van Amerongen.

The Amsterdam work is supported by FOM (Stichting Fundamenteel Onderzoek der Materie) and NWO (Nederlandse Organisatie voor Wetenschappelijk Onderzoek). The work in Orsay was supported by the Institut Francilien pour la Recherche en Atomes Froids, and by the SCALA program of the E.U.

References

- [1] J. Reichel, *Microchip traps and Bose-Einstein condensation*, Appl. Phys. B **74**, 469–487 (2002).
- [2] R. Folman, P. Krüger, J. Schmiedmayer, J. Denschlag, and C. Henkel, *Microscopic atom optics: From wires to an atom chip*, Adv. At. Mol. Opt. Phys. **48**, 263–356 (2002).
- [3] J. Fortágh and C. Zimmermann, *Magnetic microtraps for ultracold atoms*, Rev. Mod. Phys. **79**, 235 (2007).
- [4] S. Wildermuth, S. Hofferberth, I. Lesanovsky, S. Groth, P. Krüger, J. Schmiedmayer, and I. Bar-Joseph, *Sensing electric and magnetic fields with Bose-Einstein condensates*, Appl. Phys. Lett. **88**, 264103 (2006).
- [5] T. Schumm, S. Hofferberth, L. M. Andersson, S. Wildermuth, S. Groth, I. Bar-Joseph, J. Schmiedmayer, and P. Krüger, *Matter-wave interferometry in a double well on an atom chip*, Nature Phys. **1**, 57–62 (2005).
- [6] J.-B. Trebbia, J. Estève, C. I. Westbrook, and I. Bouchoule, *Experimental evidence for the breakdown of a Hartree-Fock approach in a weakly interacting Bose gas*, Phys. Rev. Lett. **97**, 250403 (2006).
- [7] J. Estève, J.-B. Trebbia, T. Schumm, A. Aspect, C. I. Westbrook, and I. Bouchoule, *Observations of density fluctuations in an elongated Bose gas: Ideal gas and quasicondensate regimes*, Phys. Rev. Lett. **96**, 130403 (2006).
- [8] A. H. van Amerongen, J. J. P. van Es, P. Wicke, K. V. Kheruntsyan, and N. J. van Druten, *Yang-Yang thermodynamics on an atom chip*, Phys. Rev. Lett. **100**, 090402 (2008).
- [9] *Special issue - atom chips: manipulating atoms and molecules with microfabricated structures*, Eur. J. Phys. D. **35** (2005).
- [10] E. H. Lieb and W. Liniger, *Exact analysis of an interacting Bose gas. i. the general solution and the ground state*, Phys. Review **130**, 1605 (1963).
- [11] E. H. Lieb, *Exact analysis of an interacting Bose gas. II. the excitation spectrum*, Phys. Rev. **130**, 1616–1624 (1963).
- [12] C. N. Yang and C. P. Yang, *Thermodynamics of a one-dimensional system of bosons with repulsive delta-function interaction*, J. Math. Phys. **10**, 1115 (1969).

- [13] W. Guerin, J.-F. Riou, J. P. Gaebler, V. Josse, P. Bouyer, and A. Aspect, *Guided quasicontinuous atom laser*, Phys. Rev. Lett **97**, 200402 (2006).
- [14] S. Hofferberth, I. Lesanovsky, B. Fischer, T. Schumm, and J. Schmiedmayer, *Non-equilibrium coherence dynamics in one-dimensional Bose gases*, Nature **449**, 324 (2007).
- [15] T. Kinoshita, T. Wenger, and D. S. Weiss, *Observation of a one-dimensional Tonks-Girardeau gas*, Science **305**, 1125–1128 (2004).
- [16] T. Kinoshita, T. Wenger, and D. S. Weiss, *Local pair correlations in one-dimensional Bose gases*, Phys. Rev. Lett. **95**, 190406 (2005).
- [17] B. Laburthe Tolra, K. M. O’Hara, J. H. Huckans, W. D. Phillips, S. L. Rolston, and J. V. Porto, *Observation of reduced three-body recombination in a correlated 1D degenerate Bose gas*, Phys. Rev. Lett. **92**, 190401 (2004).
- [18] B. Paredes, A. Widera, V. Murg, O. Mandel, S. Fölling, I. Cirac, G. V. Shlyapnikov, T. W. Hänsch, and I. Bloch, *Tonks-Girardeau gas of ultracold atoms in an optical lattice*, Nature **429**, 277–281 (2004).
- [19] H. Moritz, T. Stöferle, M. Köhl, and T. Esslinger, *Exiting collective oscillations in a trapped 1D gas*, Phys. Rev. Lett. **91**, 250402 (2003).
- [20] M. Olshanii, *Atomic scattering in the presence of an external confinement and a gas of impenetrable bosons*, Phys. Rev. Lett. **81**, 938–941 (1998).
- [21] D. Petrov, G. Shlyapnikov, and J. Walraven, *Regimes of quantum degeneracy in trapped 1D gases*, Phys. Rev. Lett. **85**, 3745 (2000).
- [22] K. V. Kheruntsyan, D. M. Gangard, P. D. Drummond, and G. V. Shlyapnikov, *Pair correlations in a finite-temperature 1D Bose gas*, Phys. Rev. Lett. **91**, 040403 (2003).
- [23] K. V. Kheruntsyan, D. M. Gangardt, P. D. Drummond, and G. V. Shlyapnikov, *Finite-temperature correlations and density profiles of an inhomogeneous interacting one-dimensional Bose gas*, Phys. Rev. A **71**, 053615 (2005).
- [24] V. N. Popov, *Functional Integrals in Quantum Field Theory and Statistical Physics* (Reidel, Dordrecht, The Netherlands, 1983).
- [25] L. Tonks, *The complete equation of state of one, two and three-dimensional gases of hard elastic spheres*, Phys. Rev. **50**, 955–963 (1936).
- [26] M. Girardeau, *Relationship between systems of impenetrable bosons and fermions in one dimension*, J. Math. Phys. **1**, 516–523 (1960).
- [27] K. Huang, *Statistical Mechanics*, 2nd ed. (John Wiley & sons, New York, 1987).

- [28] L. Lewin, *Polylogarithms and Associated Functions* (Elsevier North Holland Inc., New York, NY, USA, 1981).
- [29] G. C. Wick, *The evaluation of the collision matrix*, Phys. Rev. **80**, 268–272 (1950).
- [30] M. Yasuda and F. Shimizu, *Observation of two-atom correlation of an ultracold neon atomic beam*, Phys. Rev. Lett. **77**, 3090–3093 (1996).
- [31] S. Fölling, F. Gerbier, A. Widera, O. Mandel, T. Gericke, and I. Bloch, *Spatial quantum noise interferometry in expanding ultracold atom clouds*, Nature **434**, 481 (2005).
- [32] M. Schellekens, R. Hoppeler, A. Perrin, J. V. Gomes, D. Boiron, A. Aspect, and C. I. Westbrook, *Hanbury brown twiss effect for ultracold quantum gases*, Science **310**, 648 (2005).
- [33] C. Mora and Y. Castin, *Extension of bogoliubov theory to quasi-condensates*, Phys. Rev. A **67**, 053615 (2003).
- [34] S. Dettmer *et al.*, *Observation of phase fluctuations in elongated Bose-Einstein condensates*, Phys. Rev. Lett. **87**, 160406 (2001).
- [35] D. Hellweg, L. Cacciapuoti, M. Kottke, T. Schulte, K. Sengstock, W. Ertmer, and J. J. Arlt, *Measurement of the spatial correlation function of phase fluctuating Bose-Einstein condensates*, Phys. Rev. Lett. **91**, 010406 (2003).
- [36] S. Richard, F. Gerbier, J. H. Thywissen, M. Hugbart, P. Bouyer, and A. Aspect, *Momentum spectroscopy of 1D phase fluctuations in Bose-Einstein condensates*, Phys. Rev. Lett. **91**, 010405 (2003).
- [37] I. Shvachuk, C. Buggle, D. S. Petrov, K. Dieckmann, M. Zielonkowski, M. Kemmann, T. G. Tiecke, W. von Klitzing, G. V. Shlyapnikov, and J. T. M. Walraven, *Bose-Einstein condensation into nonequilibrium states studied by condensate focusing*, Phys. Rev. Lett. **89**, 270404 (2002).
- [38] A. H. van Amerongen, *One-dimensional Bose gas on an atom chip*, Ph.D. thesis, Universiteit van Amsterdam, 2008.
- [39] S. Hofferberth, I. Lesanovsky, T. Schumm, A. Imambekov, V. Gritsev, E. Demler, and J. Schmiedmayer, *Probing quantum and thermal noise in an interacting many-body system*, Nature Physics **4**, 489 (2008).
- [40] V. E. Korepin, N. M. Bogoliubov, and A. G. Izergin, *Quantum Inverse Scattering Method and Correlation Functions* (Cambridge University Press, Cambridge, England, 1993).
- [41] M. Takahashi, *Thermodynamics of One-Dimensional Solvable Models* (Cambridge University Press, Cambridge, England, 1999).

- [42] R. J. Baxter, *Exactly Solved Models in Statistical Mechanics* (Academic Press, 1982).
- [43] H. Bethe, *Zur theory der metalle*, *Zeitschrift für Physik* **71**, 205 (1931).
- [44] C. P. Yang, *One-dimensional system of bosons with repulsive δ -function interactions at a finite temperature t* , *Phys. Rev. A* **2**, 154–157 (1970).
- [45] I. Bouchoule, K. V. Kheruntsyan, and G. V. Shlyapnikov, *Interaction-induced crossover versus finite-size condensation in a weakly interacting trapped one-dimensional Bose gas*, *Phys. Rev. A* **75**, 031606 (2007).
- [46] J.-S. Caux and P. Calabrese, *Dynamical density-density correlations in the one-dimensional Bose gas*, *Phys. Rev. A* **74**, 031605 (2006).
- [47] A. G. Sykes, D. M. Gangardt, M. J. Davis, K. Viering, M. G. Raizen, and K. V. Kheruntsyan, *Spatial nonlocal pair correlations in a repulsive 1D Bose gas*, *Phys. Rev. Lett.* **100**, 160406 (2008).
- [48] Y. Castin, R. Dum, E. Mandonnet, A. Minguzzi, and I. Carusotto, *Coherence properties of a continuous atom laser*, *J. Modern Opt.* **47**, 2671 (2000).
- [49] P. B. Blakie and M. J. Davis, *Projected Gross-Pitaevskii equation for harmonically confined Bose gases at finite temperature*, *Phys. Rev. A* **72**, 063608 (2005).
- [50] C. Menotti and S. Stringari, *Collective oscillations of a one-dimensional trapped Bose-Einstein gas*, *Phys. Rev. A* **66**, 043610 (2002).
- [51] F. Gerbier, *Quasi-1D Bose-Einstein condensates in the dimensional crossover regime*, *Europhys. Lett.* **66**, 771 (2004).
- [52] D. S. Petrov, G. V. Shlyapnikov, and J. T. M. Walraven, *Phase-fluctuating 3D Bose-Einstein condensates in elongated traps*, *Phys. Rev. Lett.* **87**, 050404 (2001).
- [53] W. Ketterle and N. J. van Druten, *Bose-Einstein condensation of a finite number of particles trapped in one or three dimensions*, *Phys. Rev. A* **54**, 656 (1996).
- [54] A. Griffin, *Conserving and gapless approximations for an inhomogeneous Bose gas at finite temperatures*, *Phys. Rev. B* **53**, 9341 (1996).
- [55] S. Giorgini, L. P. Pitaevskii, and S. Stringari, *Condensate fraction and critical temperature of a trapped interacting Bose gas*, *Phys. Rev. A* **54**, R4633–R4636 (1996).
- [56] F. Gerbier, J. H. Thywissen, S. Richard, M. Hugbart, P. Bouyer, and A. Aspect, *Critical temperature of a trapped, weakly interacting Bose gas*, *Phys. Rev. Lett.* **92**, 030405 (2004).
- [57] M. Holzmann and W. Krauth, *Transition temperature of the homogeneous, weakly interacting Bose gas*, *Phys. Rev. Lett.* **83**, 2687–2690 (1999).

- [58] P. Arnold and G. Moore, *BEC transition temperature of a dilute homogeneous imperfect Bose gas*, Phys. Rev. Lett. **87**, 120401 (2001).
- [59] V. A. Kashurnikov, N. V. Prokof'ev, and B. V. Svistunov, *Critical temperature shift in weakly interacting Bose gas*, Phys. Rev. Lett. **87**, 120402 (2001).
- [60] T. Donner, S. Ritter, T. Bourdel, A. Til, M. Khl, and T. Esslinger, *Critical behavior of a trapped interacting Bose gas*, Science **315**, 1556 (2007).
- [61] J. Trebbia, *Etude de gaz quantiques dégénérés quasi-unidimensionnels confinés par une micro-structure*, Ph.D. thesis, Université Paris Sud - Paris XI, 2007.
- [62] C. Kittel and H. Kroemer, *Thermal Physics*, 2nd ed. (Freeman and Company, New York, NY, USA, 1980).